Biochemical Society Transactions (2020)
https://doi.org/10.1042/BST20191084

PORTLAND PRESS

Review Article

Biomolecular complex viewed by dynamic nuclear polarization solid-state NMR spectroscopy

Arnab Chakraborty[1], Fabien Deligey[1], Jenny Quach[1], Frederic Mentink-Vigier[2], Ping Wang[3] and Tuo Wang[1]

[1]Department of Chemistry, Louisiana State University, Baton Rouge, LA 70803, U.S.A; [2]National High Magnetic Field Laboratory, Tallahassee, FL 32310, U.S.A; [3]Department of Microbiology, Immunology, and Parasitology, Louisiana State University Health Sciences Center, New Orleans, LA 70112, U.S.A

Correspondence: Tuo Wang (tuowang@lsu.edu)

Solid-state nuclear magnetic resonance (ssNMR) is an indispensable tool for elucidating the structure and dynamics of insoluble and non-crystalline biomolecules. The recent advances in the sensitivity-enhancing technique magic-angle spinning dynamic nuclear polarization (MAS-DNP) have substantially expanded the territory of ssNMR investigations and enabled the detection of polymer interfaces in a cellular environment. This article highlights the emerging MAS-DNP approaches and their applications to the analysis of biomolecular composites and intact cells to determine the folding pathway and ligand binding of proteins, the structural polymorphism of low-populated biopolymers, as well as the physical interactions between carbohydrates, proteins, and lignin. These structural features provide an atomic-level understanding of many cellular processes, promoting the development of better biomaterials and inhibitors. It is anticipated that the capabilities of MAS-DNP in biomolecular and biomaterial research will be further enlarged by the rapid development of instrumentation and methodology.

Introduction

Solid-state nuclear magnetic resonance (ssNMR) spectroscopy has been successfully employed to acquire molecular insights on the structure and dynamics of many biomolecules. Most of these studies are focused on the structural determination of purified or reconstituted biomolecules such as amyloid fibrils, membrane proteins, large protein complex, ion channels and transporters, and nucleic acids [1–9]. Nevertheless, it is technically difficult to conduct high-resolution studies of biomacromolecules in their cellular environments. This limitation is the consequence of two technical issues: the inadequate resolution due to the coexistence of many heterogeneous macromolecules and the unsatisfactory sensitivity due to the low concentration of the molecules of interest. In the past decade, the sensitivity-enhancing dynamic nuclear polarization (DNP) technique has been integrated with specific isotope-labeling techniques and spectral editing approaches that efficiently attenuate spectral congestion. This has made it practicable to study protein folding, biopolymer interactions, and ligand binding using intact viruses and intact cells of bacteria, fungi, plants, and humans [10–15]. This review will summarize the technical feasibility of several emerging approaches and their applications to cellular samples as well as bio-composites. We will also elaborate on how structural restraints can be combined to conceptually comprehend the supramolecular architecture of biological constructs, which could facilitate the development of biopolymer-based materials, bio-sourced energy, and novel therapeutic agents.

Received: 1 March 2020
Revised: 17 April 2020
Accepted: 20 April 2020

Version of Record published:
7 May 2020

MAS-DNP sensitivity enhancement enables new research avenues

NMR is a low-sensitivity technique whose signal-to-noise ratios greatly depend on the gyromagnetic ratio of spins. The cutting-edge technique MAS-DNP takes advantage of the several orders of magnitude higher gyromagnetic ratio of electrons over NMR-active nuclei, such as ^{13}C or ^{1}H, to boost NMR

Biochemical Society Transactions (2020)
https://doi.org/10.1042/BST20191084

sensitivity [16–18]. An electron source, usually a stable nitroxide mono- or bi-radical, is physically or covalently incorporated into the sample, which allows the polarization of unpaired electrons to be transferred to protons under microwave irradiation (Figure 1A). The sensitivity enhancement factor ($\varepsilon_{on/off}$) is measured by taking the ratio of intensity turning the microwave radiation on to the intensity keeping it off while accounting for the depolarization effects [19]. Nitroxide-based radicals can be chemically reduced in biological samples. As demonstrated by McDermott and co-workers[20], for cells and lysates at room temperature, less than a quarter of radicals can be retained after a short time of 10 min, which corresponds to a reduction rate of 0.18 mmol/(l*min). The reaction rate is substantially slowed down to 0.12 mmol/(l*min) at a moderately low temperature of 4°C. Because the short lifetime presents a barrier, MAS-DNP experiments are usually conducted at a very low temperature of 90–110 K. The use of cryogenic temperature also increases the signal-to-noise ratios of all NMR spectra following the Boltzmann distribution and improves DNP efficiency by elongating both electron and proton relaxation times [17,21]. However, this also risks the loss of spectral resolution as a broad distribution of conformations will be trapped when the dynamic components are immobilized.

A careful choice regarding the composition of the glassy matrix (typically a mixture of water with glycerol or DMSO) and the concentration of radicals is essential because MAS-DNP efficiency is influenced by the way that radicals are dispersed in the biological medium [22–24]. A homogenous mixture of d_8-glycerol/D_2O/H_2O (60 : 30 : 10 vol%) has been widely used as the DNP juice for biomolecular samples. The formation of the glassy matrix efficiently avoids the formation of the crystalline phase, thus evading radical aggregation. Multiple water-soluble bi-radicals (with two unpaired electrons), such as TOTAPOL and AMUPol [25,26], have been widely used (Figure 1B). A recently developed, asymmetric biradical AsymPolPOK has shown meritorious performance: due to a substantial decline in the MAS-DNP buildup time, the absolute sensitivity is doubled when compared with the commercial radicals (Figure 1B,C) [27]. The DNP buildup time limits the recycle delays between two scans, which further determines the experimental time. The DNP buildup time depends on the concentration and property of radicals; it typically ranges in the scale of 2–6 s when the biomolecules are well mixed with the radicals but can be as long as tens of seconds in some challenging samples [28]. The buildup time is partially controlled by the strength of electron–electron interaction; the stronger as the shorter [29].

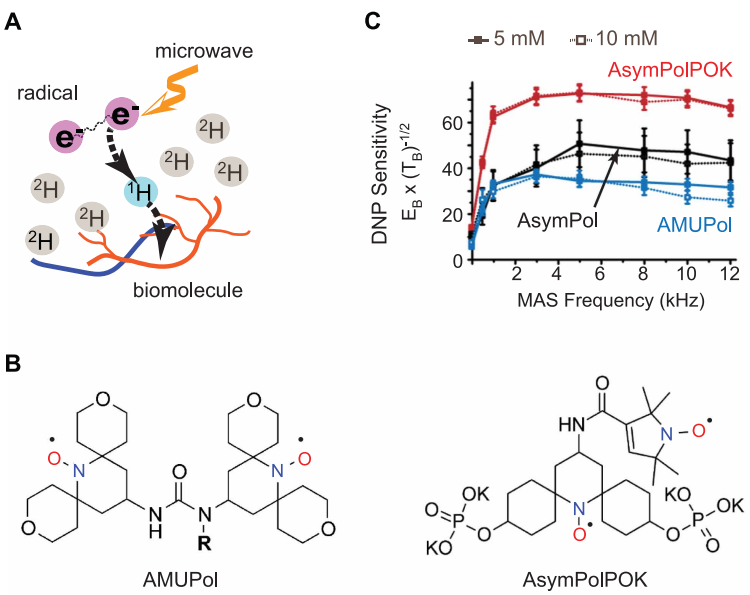

Figure 1. MAS-DNP technique boosts NMR sensitivity.

(**A**) Illustration of the MAS-DNP mechanism. (**B**) Representative structure of two bi-radicals, AMUPol, and AsymPolPOK. (**C**) Enhancement of the sensitivity of spectra collected on ^{13}C-urea at a variety of magic-angle spinning frequencies at 9.4 T and 105 K using three different bi-radicals, including AMUPol, AsymPolPOK, and AsymPol at two different concentrations (5 and 10 mM). The MAS-DNP sensitivity is quantified as the signal intensity per unit square root of time. (**B**) and (**C**) are adapted from reference [26] with copyright permission and reference [27] (an open-access article).

AsympolPOK has very strong electron dipolar and exchange interaction, which accounts for the very fast buildup even with a relatively low concentration of bi-radicals, without affecting other characteristic times [27]. In addition, there are significant efforts in covalently incorporating radicals to biomolecules at the location of interest, which provides efficient polarization of the embedded molecules and specific interaction sites [30,31]. These efforts have made MAS-DNP a versatile technique for addressing key biochemical questions with structural relevance as discussed below.

Membrane protein and protein–ligand binding

DNP-assisted ssNMR is uniquely capable of analyzing heterogeneous mixtures as it circumvents crystallization or solubilization; however, this method has its own challenges in sample preparation. It often requires chemically modified radicals [32–34] or special procedures to ensure the homogeneous mixing of biomolecules and polarizing agents. For example, because of the limited water accessibility and the impermeability of membranes towards water-soluble bi-radicals, the enhancement factors achieved on membrane protein samples (those with a reasonably low peptide-to-lipid ratio and a sufficient membrane environment) are typically below 20-fold.

In 2016, an optimized protocol that mixes radicals and membranes by direct titration has resulted in a 40–100-fold of sensitivity enhancement ($\varepsilon_{on/off}$) on a 400 MHz/263 GHz MAS-DNP instrument [22]. This approach has been successfully demonstrated on two ion channels: the influenza A M2 proton channel and an artificial designed protein channel that co-transports Zn^{2+} and H^+ ions [35]. The efficient gain of sensitivity is quantified to approach 100–160-fold by comparing MAS-DNP spectra with those collected at a higher temperature (243 K). This success has been attributed to the bimodal partitioning of radicals in the phospholipid membranes, with a surface-resided portion and a membrane-inserted fraction, which can be distinguished through the paramagnetic relaxation enhancement (PRE) effects of the unpaired electrons of bi-radicals on the signals of phospholipids [22].

At ambient temperature, quantification of the chemical shift perturbation allows us to locate the ligand-binding sites in proteins [36,37], but this approach is no longer efficient under MAS-DNP conditions due to the broader linewidth. As a result, innovative strategies have been developed to probe the protein surface and topology for binding cholesterol and carbohydrate-based ligands. In 2013, we have developed a method that relies on differential isotope-labeling (^{13}C on carbohydrate components and ^{15}N, ^{13}C on recombinantly expressed proteins) to determine the binding of a nonenzymatic loosening protein expansin to *Arabidopsis* plant cell walls [12]. DNP helps to overcome the sensitivity barrier imposed by the low functional concentration of this protein, with spectral editing techniques used to detect the protein-bound carbohydrates. Expansins are recruited to the carbohydrate junctions in which the hemicellulose xyloglucan is entrapped between multiple cellulose microfibrils or several glucan chains of a single microfibril, which turns out to be the polymer nexus being released during cell elongation [12].

Recently, Hong and co-workers [38] have developed a strategy that integrates MAS-DNP with biosynthetic ^{13}C-labeling of cholesterols from the budding yeast *Saccharomyces cerevisiae* to investigate protein–cholesterol binding in lipid bilayers. The yeast strain (RH6829) is genetically modified to produce cholesterols instead of ergosterols, and the cholesterols can be ^{13}C-labeled at alternate carbon sites using either 1- or 2-^{13}C glucose (Figure 2A). With the sensitivity enhanced by MAS-DNP, two-dimensional (2D) ^{13}C–^{13}C double-quantum filtered (DQF) spectra have explicitly resolved several cross peaks between the influenza A virus M2 protein and 1-^{13}C cholesterol in lipid bilayers. These structural constraints were combined with previous findings on the helix orientation and binding stoichiometry [39] to reveal how the M2 protein utilizes its Ile, Leu, and Phe sidechains on an annular binding site of the transmembrane helix to bind cholesterol asymmetrically through methyl–methyl and CH–π interactions (Figure 2B). These findings provide insights into the underlying mechanisms through which M2 proteins interact with membrane components, promote membrane curvatures [40–42], and facilitate the membrane scission process during viral budding and release [43].

There are tremendous efforts to covalently link mono- or bi-radicals to proteins or membranes, which, by expectation, should provide better DNP efficiency and site-specificity. Spin-labeled phosphocholine (PC) lipids have been used as the DNP polarizing agents and the constituent molecules of lipid bilayers [30,44]. The mono-radicals are tethered to the lipids at multiple sites, including the phosphate headgroup (TEMPO-PC), the middle segments (5-Doxyl PC and 7-Doxyl PC), and the terminal part of acyl chains (16-Doxyl PC). Consequently, efficient and homogenous polarization has been observed across the lipid bilayers and to membrane-embedded peptides such as a lung surfactant mimetic peptide KL_4 inserted in these membranes. In addition, site-directed incorporation of polarizing agents has also been demonstrated on the potassium channel

Biochemical Society Transactions (2020)
https://doi.org/10.1042/BST20191084

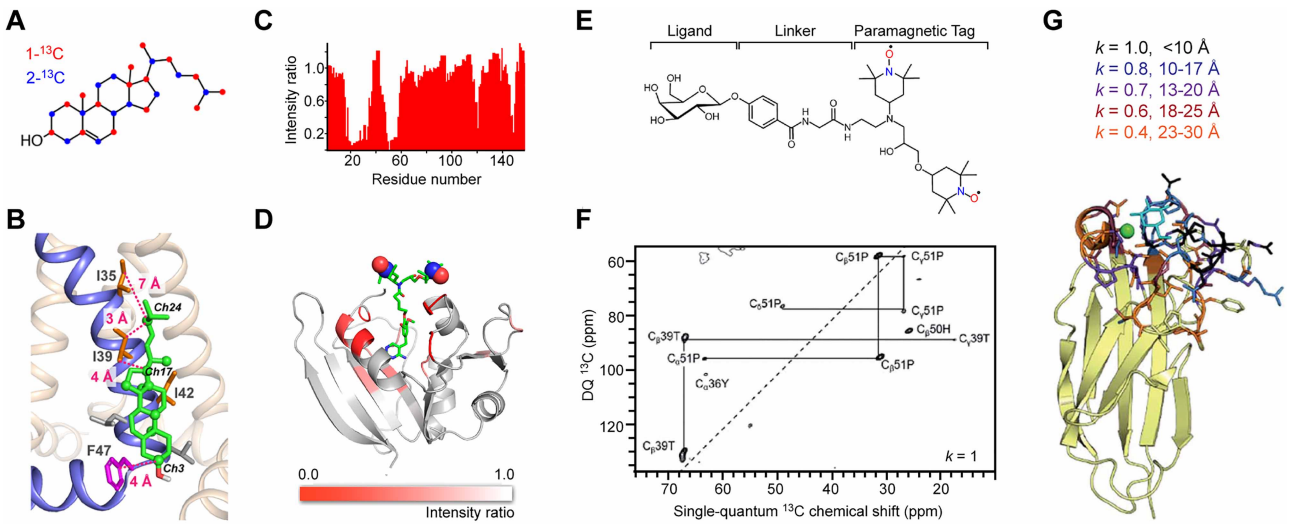

Figure 2. MAS-DNP methods for probing protein–ligand binding.

(**A**) Yeast-based ^{13}C-labeling of cholesterol using site-specifically ^{13}C-labeled glucose. The labeled carbon sites on cholesterol are in red and blue for cholesterols produced from 1-^{13}C and 2-^{13}C glucose molecules, respectively. (**B**) A structural model of a cholesterol molecule bound to the influenza M2 proteins. The key Ile and Phe residues, as well as their distances to cholesterol carbons, are shown. (**C**) Signal bleaching quantified in solution ^{1}H–^{15}N HSQC spectra due to the binding of radicals to dihydrofolate reductase. (**D**) A model of *E. coli* dihydrofolate reductase with DNP bleaching information represented by the intensity ratios of ^{13}C–^{13}C DARR spectra collected on two samples containing either bound radicals or exogenous radicals. (**E**) Scheme for incorporating a carbohydrate ligand to a paramagnetic tag for selective DNP. (**F**) Selective DNP ^{13}C–^{13}C INADEQUATE difference spectrum of LecA obtained using $k = 1$: only the tightly bound residues are observed. (**G**) Sideview of LecA. Residues observed using selective DNP are highlighted, with the corresponding k values given. (**A–D**) are adapted from references [38,51] with copyright permission. (**E–G**) are adapted from reference [31], an open-access article.

KcsA, the antibiotics gramicidin, and the sensory rhodopsin [45–47]. Targeted DNP has also been used to investigate the interaction between a radical-labeled ligand with a 20 kDa protein (Bcl-x_L) at a low concentration in crude cell lysates [48].

Because radicals are paramagnetic species, spins in their spatial vicinity experience faster NMR relaxation, which leads to line broadening and intensity suppression [49,50]. The signal quenching, also called paramagnetic bleaching, can be quantified when the radical is directly bound to a protein (Figure 2C). This technique has been applied to determine the distance of a combined ligand-radical to a reductase in *Escherichia coli* bacteria [51]. A comparison of the DNP spectra collected on two samples, one with a radical bound to the protein with high affinity and the other with the solvent-bearing AMUPol as a reference, has pinpointed the protein surface that is responsible for binding the target (Figure 2D).

Signal bleaching has also been employed to improve resolution when probing protein–ligand binding. This process has been successfully achieved by functionalizing the ligand (for example, carbohydrates) with a polarizing agent (TOTAPOL) covalently linked through a phenylglycine linker (Figure 2E) [31]. The conceptual setup is consistent with the studies of the *E. coli* reductase as discussed above, with additional assistance from difference spectroscopy [52,53] in which the spectrum measured using the paramagnetically tagged sample is subtracted from a reference spectrum measured on a sample only containing radicals homogenously distributed in the solvent. A selective factor k is applied to the spectrum of the paramagnetically tagged sample before spectral subtraction, which renders selective DNP mimicking an atomic-resolution microscope with adjustable magnification: only the tightly bound residues (<10 Å) can be observed in the difference spectrum when $k = 1$ is applied (Figure 2F), and the observable region gradually expands to 30 Å with a decreasing k value. This method has been applied to the study of a galactose-specific lectin LecA [31]. The spectral subtraction provides unprecedented resolution for unambiguously locating the carbohydrate-binding spots on LecA (Figure 2G). This method requires no prior knowledge of the binding site and has no limitation on the protein size.

Protein structure in cellular fractions and intact cells

The magnificent sensitivity has made DNP a suitable tool for studying highly diluted biomolecules in cellular fractions or whole cells, which are otherwise 'invisible'. In 2015, the type IV secretion system core complex (T4SScc), a megadalton protein complex, has been investigated in the cell envelope fractions of *E. coli* [54]. In the cellular system, this protein maintains its correct folding and assembles into a structure that is consistent with the X-ray crystallography results. Similarly, a protocol has been established to study protein folding in cellular lysates, which combines different labeling schemes to produce a sample containing NMR-active prion proteins and an NMR-silent cellular environment (Figure 3A) [13,55]. The technique was employed to determine the folding of an intrinsically disordered region of the yeast prion protein Sup35. The Sup35 fibrils were found to be restructured and different from *in vitro* templated assemblies [13].

Intact human cells have remained as a challenging system for DNP ssNMR, especially for the optimization of radicals and experimental conditions. In 2019, an original protocol has been designed to examine protein structures in mammalian cells. This approach comprises of three steps: isotope-labeling the protein of interest, delivery of the protein into cells by electroporation techniques followed by a cell stimulus, and the introduction of bi-radicals for DNP measurement [56]. The cell integrity and biradical distribution have been simultaneously monitored with microscopy techniques. It is found that the model protein ubiquitin has remained correctly folded after delivery into the HeLa cell [56]. In the same year, another study has quantified the chemical reduction effect of nitroxide bi-radicals in *E. coli* pellets, suspensions, and lysates. Treatment of the cell using *N*-ethylmaleimide could neutralize pools of redox-active cysteines, suppress nitroxide reduction, and prolong the lifetime of radicals while adding potassium ferricyanide effectively re-oxidizes the reacted radicals back into their active state [20]. In 2018, a trimodal polarizing agent TotaFAM has been introduced, which contains a biradical, a targeting cell-penetrating peptide, and a fluorophore for tracking the localization of radicals in the cell (Figure 3B) [14]. The radical uptake is efficient in HEK293F cells (Figure 3C) and a high enhancement of 63-fold of the cellular signals was achieved using a low radical concentration (2.7 mM). In comparison, commercial radicals require a much higher concentration (20 mM) to reach a comparable performance (Figure 3D). These ground-breaking advances have paved the way for understanding the molecular structure, functional mechanisms, and drug inhibition [57] of protein machinery and other biomolecules within their cellular environments.

Biopolymer packing in fungal and plant cell walls

There is a growing interest in characterizing cell walls of plants and microbes because these protective armors are the resources of new energy and the targets of antimicrobial therapeutic compounds [58–60]. During the past years, many organisms have been investigated using ssNMR, including the cell walls of many plants, pathogenic fungi, microalgae, and bacteria [61–75]. The highly rigid and semi-crystalline components, for example, cellulose microfibrils in plants and chitin in fungi, are capable of retaining decent resolution under cryogenic conditions [11,12,76], which has made the carbohydrate-rich cell walls a preferred system for DNP investigations. In addition, radicals mainly accumulate in the cell walls due to a high binding affinity to the

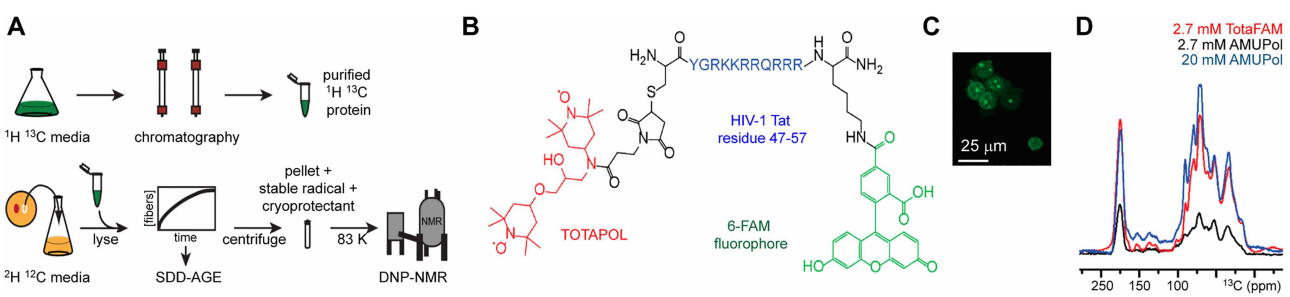

Figure 3. Cellular MAS-DNP of protein structure.

(**A**) Preparation of proteins at endogenous levels for MAS-DNP in biological environments. (**B**) Chemical structure of the trimodal polarizing agent TotaFAM. (**C**) A fluorescent image confirms the cellular uptake of TotaFAM. (**D**) 1D ^{13}C spectra of HEK293F cells at <6 K using different radicals. Figures are adapted from references [13,14] with copyright permission.

Biochemical Society Transactions (2020)
https://doi.org/10.1042/BST20191084

carbohydrate components such as the peptidoglycan in bacteria and cellulose in plants [77–79]. We can either selectively detect the cell wall molecules using a low concentration of radicals (for example, 5 mM) or observe other cellular components by bleaching the cell wall signals using a saturated concentration of radicals (for example, 60 mM) [79]. Moreover, NMR fingerprints of the highly polymerized polysaccharides in the cell wall are uniquely different from those of intracellular and metabolic carbohydrates or other molecules (e.g. proteins and nucleic acids) [23]; therefore, cell walls are spectroscopically distinguishable from other cellular components.

Recently, we have been elucidating the structural organization of cell walls in several fungal pathogens, starting from a model fungus *Aspergillus fumigatus* [11] and progressively outspreading to other yeasts as well as molds. A 30-fold of sensitivity enhancement ($\varepsilon_{on/off}$) allows us to highlight the highly polymorphic nature of biomolecules in intact fungal cell walls and efficiently probe their sub-nanometer packing. Despite its low abundance (~10% of the dry mass of *A. fumigatus* cell walls), chitin exists in three major forms as shown by the peak multiplicity of 2D ^{15}N–^{13}C correlation spectra (Figure 4A). These signals deviate from the chemical shifts of model chitin crystallites from fungi or other sources [80,81]. This unexpected level of structural polymorphism has been attributed to the complicated patterns of hydrogen-bonding (through the amide and carbonyl groups) that form parallel, antiparallel, and mixed ways of packing in chitin microfibrils [82,83]. The different forms are extensively mixed in individual microfibrils as evidenced by inter-form correlations using the 2D ^{15}N–^{15}N proton assisted recoupling (PAR) experiment [84–86]. When associated with difference spectroscopy, MAS-DNP has increased both spectral resolution and resolution so that many chitin–glucan interactions can be identified, unveiling a mechanical framework of tightly associated chitin and α-1,3-glucans. This is a novel feature that had never been discovered before [11]. Integrated with the conventional NMR data collected at room temperature, the chitin-α-1,3-glucan scaffold is further found to reside in a soft matrix of β-glucans and capped by a glycoprotein-rich shell [11].

When applied to the plant secondary cell walls, MAS-DNP is employed to probe the physical contacts between multiple polysaccharides and the aromatic polymer lignin, which is a polymer interface with a low occurrence. Assisted by dipolar and frequency filters as well as a mechanical shutter that regulates microwave on the millisecond timescale [87], we have cleanly selected the aromatic signals from lignin and further determined the composition of polysaccharides in the vicinity. Contradictory to the prevailing knowledge, cellulose is found to lack interactions with lignin in maize stems because the signals from the internal and surface

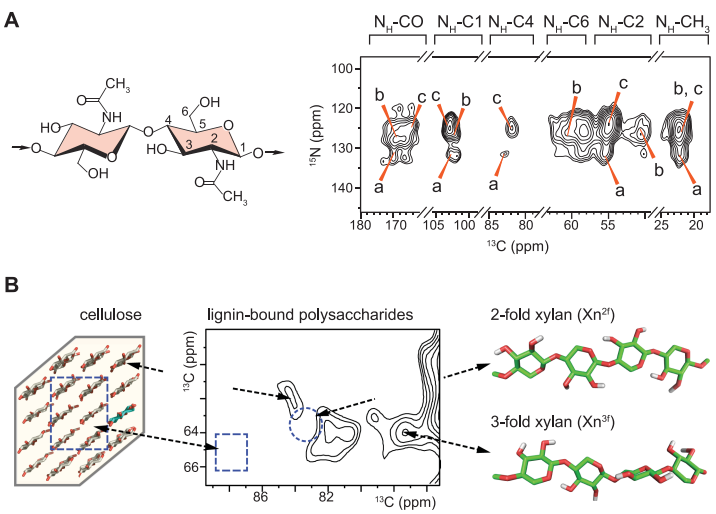

Figure 4. Polysaccharide structure and polymer binding in plant and fungal cell walls.

(**A**) Representative structure and MAS-DNP spectra of chitin in cell walls of intact *A. fumigatus*. Three major types of chitin signals have been resolved (Types a–c). (**B**) The aromatic-edited spectrum of maize stems shows the signals of lignin-bound carbohydrates. Arrows and black dotted lines connect the spectral regions with polysaccharide structures. The dashline circle and rectangle on the spectrum highlight the missing signals of the carbohydrate components that are far from lignin. Figures are adapted from references [10,11], which are open-access publications.

glucan chains in the microfibrils are either missing or weak (Figure 4B) [10]. The polysaccharide interactor of lignin is found to be the hemicellulose xylan, which relies on its twisted 3-fold conformers (3 residues per helical turn) to bind lignin and uses the 2-fold flat-ribbon domains to bind cellulose microfibrils [10]. The molecular information of the lignin–carbohydrate interface provides an understanding of the polymer interactions underlying the nanoscale architecture of this bio-complex, which has revised the structural concepts of lignocellulosic biomass. In addition, MAS-DNP has been employed to screen the carbohydrate and lignin constituents of poplar and its genetic variants following chemical treatments, which will aid the improvement of biomass conversion technology [88,89].

Beyond these studies, there are many other DNP investigations focused on complex biosystems, for example, the DNA and coat proteins of the filamentous phage Pf1 in an intact virus, the supramolecular assembly of HIV capsid, the peptidoglycans of *Bacillus subtilis* bacterial cell walls, the nucleic acids in bones, the post-translational collagen modification in muscle cell-extracellular matrix, and the interfaces of biominerals [15,79,90–96]. The scope of MAS-DNP should be substantially broadened by high-field DNP that provides better resolution, the natural-abundance technique that eliminates the need for isotope-enrichment, and the analytical software for spectral and structural comparisons [97–101]. These efforts have the potential for revolutionizing biomolecular and biomaterial research.

Perspectives

- *Importance of the field*: MAS-DNP has vastly broadened the horizon of solid-state NMR spectroscopy and enabled the atomic-level view of polymorphic biomolecules in their native cellular environments. The structural insights of protein machinery and structural carbohydrates also provide an in-depth understanding of many cellular processes to guide the development of functional biomaterials, bio-renewable energy, and novel inhibitors.

- *Summaries of the current thinking*: The molecular structure and binding interactions of many carbohydrate- or protein-based biopolymers have been successfully investigated using biomolecular mixtures, cellular fractions, and intact cells. Due to the complex nature of cellular polymers, MAS-DNP investigations should be coupled with selective labeling or site-directed polarization technology to efficiently alleviate spectral congestion.

- *Future directions*: The rapid development of high-field and fast-MAS-DNP as well as natural-abundance approaches have established a new avenue of biochemical research, especially for the complex biosystems with a high demand for resolution or the biomedical samples that are difficult to replicate *in vitro*.

Competing Interests

The authors declare that there are no competing interests associated with the manuscript.

Acknowledgment

This work was supported by the National Institutes of Health grant AI149289. T.W. thanks the support of the Center for Lignocellulose Structure and Formation, an Energy Frontier Research Center funded by the US Department of Energy, Office of Science, Basic Energy Sciences under award number DE-SC0001090 for solid-state NMR studies of plant cell walls. The National High Magnetic Field Laboratory is supported by National Science Foundation through NSF/DMR-1644779 and the State of Florida. The MAS-DNP program at NHMFL is funded by the NIH P41 GM122698.

Abbreviations

MAS, magic-angle spinning; MAS-DNP, magic-angle spinning dynamic nuclear polarization; PRE, paramagnetic relaxation enhancement; ssNMR, solid-state nuclear magnetic resonance.

References

1 McDermott, A. (2009) Structure and dynamics of membrane proteins by magic angle spinning solid-state NMR. *Annu. Rev. Biophys.* **38**, 385–403 https://doi.org/10.1146/annurev.biophys.050708.133719

2 Marchanka, A., Simon, B., Althoff-Ospelt, G. and Carlomagno, T. (2015) RNA structure determination by solid-state NMR spectroscopy. *Nat. Commun.* **6**, 7024 https://doi.org/10.1038/ncomms8024

3 Meier, B.H., Riek, R. and Bockmann, A. (2017) Emerging structural understanding of amyloid fibrils by solid-state NMR. *Trends Biochem. Sci.* **42**, 777–787 https://doi.org/10.1016/j.tibs.2017.08.001

4 Comellas, G. and Rienstra, C.M. (2013) Protein structure determination by magic-angle spinning solid-state NMR, and insights into the formation, structure, and stability of amyloid fibrils. *Annu. Rev. Biophys.* **42**, 515–536 https://doi.org/10.1146/annurev-biophys-083012-130356

5 Mandala, V.S., Williams, J.K. and Hong, M. (2018) Structure and dynamics of membrane proteins from solid-state NMR. *Annu. Rev. Biophys.* **47**, 201–222 https://doi.org/10.1146/annurev-biophys-070816-033712

6 Quinn, C.M. and Polenova, T. (2017) Structural biology of supramolecular assemblies by magic-angle spinning NMR spectroscopy. *Q. Rev. Biophys.* **50**, e1 https://doi.org/10.1017/S0033583516000159

7 Ader, C., Schneider, R., Seidel, K., Etzkorn, M. and Baldus, M. (2007) Magic-angle-spinning NMR spectroscopy applied to small molecules and peptides in lipid bilayers. *Biochem. Soc. Trans.* **35**, 991–995 https://doi.org/10.1042/BST0350991

8 Middleton, D.A. (2007) Solid-state NMR spectroscopy as a tool for drug design: from membrane-embedded targets to amyloid fibrils. *Biochem. Soc. Trans.* **35**, 985–990 https://doi.org/10.1042/BST0350985

9 Uluca, B., Viennet, T., Petrovic, D., Shaykhalishahi, H., Weirich, F., Gonulalan, A. et al. (2018) DNP-enhanced MAS NMR: a tool to snapshot conformational ensembles of alpha-synuclein in different states. *Biophys. J.* **114**, 1614–1623 https://doi.org/10.1016/j.bpj.2018.02.011

10 Kang, X., Kirui, A., Dickwella Widanage, M.C., Mentink-Vigier, F., Cosgrove, D.J. and Wang, T. (2019) Lignin-polysaccharide interactions in plant secondary cell walls revealed by solid-state NMR. *Nat. Commun.* **10**, 347 https://doi.org/10.1038/s41467-018-08252-0

11 Kang, X., Kirui, A., Muszynski, A., Widanage, M.C.D., Chen, A., Azadi, P. et al. (2018) Molecular architecture of fungal cell walls revealed by solid-state NMR. *Nat. Commun.* **9**, 2747 https://doi.org/10.1038/s41467-018-05199-0

12 Wang, T., Park, Y.B., Caporini, M.A., Rosay, M., Zhong, L.H., Cosgrove, D.J. et al. (2013) Sensitivity-enhanced solid-state NMR detection of expansin's target in plant cell walls. *Proc. Natl. Acad. Sci. U.S.A.* **110**, 16444–16449 https://doi.org/10.1073/pnas.1316290110

13 Frederick, K.K., Michaelis, V.K., Corzilius, B., Ong, T.C., Jacavone, A.C., Griffin, R.G. et al. (2015) Sensitivity-enhanced NMR reveals alterations in protein structure by cellular milieus. *Cell* **163**, 620–628 https://doi.org/10.1016/j.cell.2015.09.024

14 Albert, B.J., Gao, C.K., Sesti, E.L., Saliba, E.P., Alaniva, N., Scott, F.J. et al. (2018) Dynamic nuclear polarization nuclear magnetic resonance in human cells using fluorescent polarizing agents. *Biochemistry* **57**, 4741–4746 https://doi.org/10.1021/acs.biochem.8b00257

15 Sergeyev, I.V., Itin, B., Rogawski, R., Day, L.A. and McDermott, A.E. (2017) Efficient assignment and NMR analysis of an intact virus using sequential side-chain correlations and DNP sensitization. *Proc. Natl. Acad. Sci. U.S.A.* **114**, 5171–5176 https://doi.org/10.1073/pnas.1701484114

16 Mentink-Vigier, F., Akbey, U., Oschkinat, H., Vega, S. and Feintuch, A. (2015) Theoretical aspects of magic angle spinning - dynamic nuclear polarization. *J. Magn. Reson.* **258**, 102–120 https://doi.org/10.1016/j.jmr.2015.07.001

17 Ni, Q.Z., Daviso, E., Can, T.V., Markhasin, E., Jawla, S.K., Swager, T.M. et al. (2013) High frequency dynamic nuclear polarization. *Acc. Chem. Res.* **46**, 1933–1941 https://doi.org/10.1021/ar300348n

18 Rossini, A.J., Zagdoun, A., Lelli, M., Lesage, A., Coperet, C. and Emsley, L. (2013) Dynamic nuclear polarization surface enhanced NMR spectroscopy. *Acc. Chem. Res.* **46**, 1942–1951 https://doi.org/10.1021/ar300322x

19 Hediger, S., Lee, D., Mentink-Vigier, F. and De Paepe, G. (2018) MAS-DNP enhancements: hyperpolarization, depolarization, and absolute sensitivity. *eMagRes* **7**, 105–116 https://doi.org/10.1002/9780470034590.emrstm1559

20 McCoy, K.M., Rogawski, R., Stovicek, O. and McDermott, A.E. (2019) Stability of nitroxide biradical TOTAPOL in biological samples. *J. Magn. Reson.* **303**, 115–120 https://doi.org/10.1016/j.jmr.2019.04.013

21 Thurber, K.R., Yau, W.M. and Tycko, R. (2010) Low-temperature dynamic nuclear polarization at 9.4 T with a 30 mW microwave source. *J. Magn. Reson.* **204**, 303–313 https://doi.org/10.1016/j.jmr.2010.03.016

22 Liao, S.Y., Lee, M., Wang, T., Sergeyev, I.V. and Hong, M. (2016) Efficient DNP NMR of membrane proteins: sample preparation protocols, sensitivity, and radical location. *J. Biomol. NMR* **64**, 223–237 https://doi.org/10.1007/s10858-016-0023-3

23 Kirui, A., Dickwella Widanage, M.C., Mentink-Vigier, F., Wang, P., Kang, X. and Wang, T. (2019) Preparation of fungal and plant materials for structural elucidation using dynamic nuclear polarization solid-state NMR. *J. Vis. Exp.* **144**, e59152 https://doi.org/10.3791/59152

24 Takahashi, H., Fernandez-de-Alba, C., Lee, D., Maurel, V., Gambarelli, S., Bardet, M. et al. (2014) Optimization of an absolute sensitivity in a glassy matrix during DNP-enhanced multidimensional solid-state NMR experiments. *J. Magn. Reson.* **239**, 91–99 https://doi.org/10.1016/j.jmr.2013.12.005

25 Song, C.S., Hu, K.N., Joo, C.G., Swager, T.M. and Griffin, R.G. (2006) TOTAPOL: a biradical polarizing agent for dynamic nuclear polarization experiments in aqueous media. *J. Am. Chem. Soc.* **128**, 11385–11390 https://doi.org/10.1021/ja061284b

26 Sauvee, C., Rosay, M., Casano, G., Aussenac, F., Weber, R.T., Ouari, O. et al. (2013) Highly efficient, water-soluble polarizing agents for dynamic nuclear polarization at high frequency. *Angew. Chem. Int. Ed.* **52**, 10858–10861 https://doi.org/10.1002/anie.201304657

27 Mentink-Vigier, F., Marin-Montesinos, I., Jagtap, A.P., Halbritter, T., van Tol, J., Hediger, S. et al. (2018) Computationally assisted design of polarizing agents for dynamic nuclear polarization enhanced NMR: the AsymPol family. *J. Am. Chem. Soc.* **140**, 11013–11019 https://doi.org/10.1021/jacs.8b04911

28 Linden, A.H., Lange, S., Franks, W.T., Akbey, U., Specker, E., van Rossum, B.J. et al. (2011) Neurotoxin II bound to acetylcholine receptors in native membranes studied by dynamic nuclear polarization NMR. *J. Am. Chem. Soc.* **133**, 19266–19269 https://doi.org/10.1021/ja206999c

29 Mentink-Vigier, F., Vega, S. and De Paepe, G. (2017) Fast and accurate MAS-DNP simulations of large spin ensembles. *Phys. Chem. Chem. Phys.* **19**, 3506–3522 https://doi.org/10.1039/C6CP07881H

30 Smith, A.N., Caporini, M.A., Fanucci, G.E. and Long, J.R. (2015) A method for dynamic nuclear polarization enhancement of membrane proteins. *Angew. Chem. Int. Ed. Engl.* **54**, 1542–1546 https://doi.org/10.1002/anie.201410249

31 Marin-Montesinos, I., Goyard, D., Gillon, E., Renaudet, O., Imberty, A., Hediger, S. et al. (2019) Selective high-resolution DNP-enhanced NMR of biomolecular binding sites. *Chem. Sci.* **10**, 3366–3374 https://doi.org/10.1039/C8SC05696J

32 Fernandez-de-Alba, C., Takahashi, H., Richard, A., Chenavier, Y., Dubois, L., Maurel, V. et al. (2015) Matrix-free DNP-enhanced NMR spectroscopy of liposomes using a lipid-anchored biradical. *Chem. Eur. J.* **21**, 4512–4517 https://doi.org/10.1002/chem.201404588
33 Lim, B.J., Ackermann, B.E. and Debelouchina, G.T. (2019) Targetable tetrazine-based dynamic nuclear polarization agents for biological systems. *ChemBioChem*. https://doi.org/10.1002/cbic.201900609
34 Salnikov, E.S., Abel, S., Karthikeyan, G., Karoui, H., Aussenac, F., Tordo, P. et al. (2017) Dynamic nuclear polarization/solid-state NMR spectroscopy of membrane polypeptides: free-radical optimization for matrix-free lipid bilayer samples. *ChemPhysChem* **18**, 2103–2113 https://doi.org/10.1002/cphc.201700389
35 Joh, N.H., Wang, T., Bhate, M.P., Acharya, R., Wu, Y.B., Grabe, M. et al. (2014) De novo design of a transmembrane Zn^{2+}-transporting four-helix bundle. *Science* **346**, 1520–1524 https://doi.org/10.1126/science.1261172
36 Williamson, M.P. (2013) Using chemical shift perturbation to characterise ligand binding. *Prog. Nucl. Magn. Reson Spectrosc.* **73**, 1–16 https://doi.org/10.1016/j.pnmrs.2013.02.001
37 Charlton, A.J., Baxter, N.J., Khan, M.L., Moir, A.J.G., Haslam, E., Davies, A.P. et al. (2002) Polyphenol/peptide binding and precipitation. *J. Agric. Food Chem.* **50**, 1593–1601 https://doi.org/10.1021/jf010897z
38 Elkins, M.R., Sergeyev, I.V. and Hong, M. (2018) Determining cholesterol binding to membrane proteins by cholesterol ^{13}C labeling in yeast and dynamic nuclear polarization NMR. *J. Am. Chem. Soc.* **140**, 15437–15449 https://doi.org/10.1021/jacs.8b09658
39 Elkins, M.R., Williams, J.K., Gelenter, M.D., Dai, P., Kwon, B., Sergeyev, I.V. et al. (2017) Cholesterol-binding site of the influenza M2 protein in lipid bilayers from solid-state NMR. *Proc. Natl. Acad. Sci. U.S.A.* **114**, 12946–12951 https://doi.org/10.1073/pnas.1715127114
40 Schmidt, N.W., Mishra, A., Wang, J., DeGrado, W.F. and Wong, G.C.L. (2013) Influenza virus A M2 protein generates negative Gaussian membrane curvature necessary for budding and scission. *J. Am. Chem. Soc.* **135**, 13710–13719 https://doi.org/10.1021/ja400146z
41 Wang, T., Cady, S.D. and Hong, M. (2012) NMR determination of protein partitioning into membrane domains with different curvatures and application to the influenza M2 peptide. *Biophys. J.* **102**, 787–794 https://doi.org/10.1016/j.bpj.2012.01.010
42 Wang, T. and Hong, M. (2015) Investigation of the curvature induction and membrane localization of the influenza virus M2 protein using static and off-magic-angle spinning solid-state nuclear magnetic resonance of oriented bicelles. *Biochemistry* **54**, 2214–2226 https://doi.org/10.1021/acs.biochem.5b00127
43 Rossman, J.S., Jing, X.H., Leser, G.P. and Lamb, R.A. (2010) Influenza virus M2 protein mediates ESCRT-independent membrane scission. *Cell* **142**, 902–913 https://doi.org/10.1016/j.cell.2010.08.029
44 Smith, A.N., Twahir, U.T., Dubroca, T., Fanucci, G.E. and Long, J.R. (2016) Molecular rationale for improved dynamic nuclear polarization of biomembranes. *J. Phys. Chem. B* **120**, 7880–7888 https://doi.org/10.1021/acs.jpcb.6b02885
45 van der Cruijsen, E.A.W., Koers, E.J., Sauvee, C., Hulse, R.E., Weingarth, M., Ouari, O. et al. (2015) Biomolecular DNP-supported NMR spectroscopy using site-directed spin labeling. *Chem. Eur. J.* **21**, 12971–12977 https://doi.org/10.1002/chem.201501376
46 Wylie, B.J., Dzikovski, B.G., Pawsey, S., Caporini, M., Rosay, M., Freed, J.H. et al. (2015) Dynamic nuclear polarization of membrane proteins: covalently bound spin-labels at protein–protein interfaces. *J. Biomol. NMR* **61**, 361–367 https://doi.org/10.1007/s10858-015-9919-6
47 Voinov, M.A., Good, D.B., Ward, M.E., Milikisiyants, S., Marek, A., Caporini, M.A. et al. (2015) Cysteine-specific labeling of proteins with a nitroxide biradical for dynamic nuclear polarization NMR. *J. Phys. Chem. B* **119**, 10180–10190 https://doi.org/10.1021/acs.jpcb.5b05230
48 Viennet, T., Viegas, A., Kuepper, A., Arens, S., Gelev, V., Petrov, O. et al. (2016) Selective protein hyperpolarization in cell lysates using targeted dynamic nuclear polarization. *Angew. Chem. Int. Ed.* **55**, 10746–10750 https://doi.org/10.1002/anie.201603205
49 Sengupta, I., Nadaud, P.S. and Jaroniec, C.P. (2013) Protein structure determination with paramagnetic solid-state NMR spectroscopy. *Acc. Chem. Res.* **46**, 2117–2126 https://doi.org/10.1021/ar300360q
50 Corzilius, B., Andreas, L.B., Smith, A.A., Ni, Q.Z. and Griffin, R.G. (2014) Paramagnet induced signal quenching in MAS-DNP experiments in frozen homogeneous solutions. *J. Magn. Reson.* **240**, 113–123 https://doi.org/10.1016/j.jmr.2013.11.013
51 Rogawski, R., Sergeyev, I.V., Zhang, Y., Tran, T.H., Li, Y.J., Tong, L. et al. (2017) NMR signal quenching from bound biradical affinity reagents in DNP samples. *J. Phys. Chem. B* **121**, 10770–10781 https://doi.org/10.1021/acs.jpcb.7b08274
52 Wang, T., Williams, J.K., Schmidt-Rohr, K. and Hong, M. (2015) Relaxation-compensated difference spin diffusion NMR for detecting ^{13}C–^{13}C long-range correlations in proteins and polysaccharides. *J. Biomol. NMR* **61**, 97–107 https://doi.org/10.1007/s10858-014-9889-0
53 Wang, T., Chen, Y.N., Tabuchi, A., Cosgrove, D.J. and Hong, M. (2016) The target of β-expansin EXPB1 in maize cell walls from binding and solid-state NMR studies. *Plant Physiol.* **172**, 2107–2119 https://doi.org/10.1104/pp.16.01311
54 Kaplan, M., Cukkemane, A., van Zundert, G.C.P., Narasimhan, S., Daniels, M., Mance, D. et al. (2015) Probing a cell-embedded megadalton protein complex by DNP-supported solid-state NMR. *Nat. Methods* **12**, 649–652 https://doi.org/10.1038/nmeth.3406
55 Frederick, K.K., Michaelis, V.K., Caporini, M.A., Andreas, L.B., Debelouchina, G.T., Griffin, R.G. et al. (2017) Combining DNP NMR with segmental and specific labeling to study a yeast prion protein strain that is not parallel in-register. *Proc. Natl. Acad. Sci. U.S.A.* **114**, 3642–3647 https://doi.org/10.1073/pnas.1619051114
56 Narasimhan, S., Scherpe, S., Paioni, A.L., van der Zwan, J., Folkers, G.E., Ovaa, H. et al. (2019) DNP-supported solid-state NMR spectroscopy of proteins inside mammalian cells. *Angew. Chem. Int. Ed.* **58**, 12969–12973 https://doi.org/10.1002/anie.201903246
57 Schlagnitweit, J., Sandoz, S.F., Jaworski, A., Guzzetti, I., Aussenac, F., Carbajo, R.J. et al. (2019) Observing an antisense drug complex in intact human cells by in-cell NMR spectroscopy. *ChemBioChem* **20**, 2474–2478 https://doi.org/10.1002/cbic.201900297
58 Cosgrove, D.J. (2001) Wall structure and wall loosening. A look backwards and forwards. *Plant Physiol.* **125**, 131–134 https://doi.org/10.1104/pp.125.1.131
59 Brown, G.D., Denning, D.W., Gow, N.A.R., Levitz, S.M., Netea, M.G. and White, T.C. (2012) Hidden killers: human fungal infections. *Sci. Transl. Med.* **4**, 165rv13 https://doi.org/10.1126/scitranslmed.3004404
60 Fontaine, T., Mouyna, I., Hartland, R.P., Paris, S. and Latge, J.P. (1997) From the surface to the inner layer of the fungal cell wall. *Biochem. Soc. Trans.* **25**, 194–199 https://doi.org/10.1042/bst0250194
61 Nygaard, R., Romaniuk, J.A.H., Rice, D.M. and Cegelski, L. (2015) Spectral snapshots of bacterial cell-wall composition and the influence of antibiotics by whole-cell NMR. *Biophys. J.* **108**, 1380–1389 https://doi.org/10.1016/j.bpj.2015.01.037
62 Arnold, A.A., Bourgouin, J.P., Genard, B., Warschawski, D.E., Tremblay, R. and Marcotte, I. (2018) Whole cell solid-state NMR study of *Chlamydomonas reinhardtii* microalgae. *J. Biomol. NMR* **70**, 123–131 https://doi.org/10.1007/s10858-018-0164-7

63 Chatterjee, S., Prados-Rosales, R., Itin, B., Casadevall, A. and Stark, R.E. (2015) Solid-state NMR reveals the carbon-based molecular architecture of *Cryptococcus neoformans* fungal eumelanins in the cell wall. *J. Biol. Chem.* **290**, 13779–13790 https://doi.org/10.1074/jbc.M114.618389

64 Chatterjee, S., Prados-Rosales, R., Tan, S., Phan, V.C., Chrissian, C., Itin, B. et al. (2018) The melanization road more traveled by: precursor substrate effects on melanin synthesis in cell-free and fungal cell systems. *J. Biol. Chem.* **293**, 20157–20168 https://doi.org/10.1074/jbc.RA118.005791

65 Terrett, O.M., Lyczakowski, J.J., Yu, L., Iuga, D., Franks, W.T., Brown, S.P. et al. (2019) Molecular architecture of softwood revealed by solid-state NMR. *Nat. Commun.* **10**, 4978 https://doi.org/10.1038/s41467-019-12979-9

66 Simmons, T.J., Mortimer, J.C., Bernardinelli, O.D., Poppler, A.C., Brown, S.P., deAzevedo, E.R. et al. (2016) Folding of xylan onto cellulose fibrils in plant cell walls revealed by solid-state NMR. *Nat. Commun.* **7**, 13902 https://doi.org/10.1038/ncomms13902

67 Wang, T., Salazar, A., Zabotina, O.A. and Hong, M. (2014) Structure and dynamics of *Brachypodium* primary cell wall polysaccharides from two-dimensional ^{13}C solid-state nuclear magnetic resonance spectroscopy. *Biochemistry* **53**, 2840–2854 https://doi.org/10.1021/bi500231b

68 Wang, T., Yang, H., Kubicki, J.D. and Hong, M. (2016) Cellulose structural polymorphism in plant primary cell walls investigated by high-field 2D solid-state NMR spectroscopy and density functional theory calculations. *Biomacromolecules* **17**, 2210–2222 https://doi.org/10.1021/acs.biomac.6b00441

69 Phyo, P., Wang, T., Kiemle, S.N., O'Neill, H., Pingali, S.V., Hong, M. et al. (2017) Gradients in wall mechanics and polysaccharides along growing inflorescence stems. *Plant Physiol.* **175**, 1593–1607 https://doi.org/10.1104/pp.17.01270

70 Phyo, P., Wang, T., Xiao, C.W., Anderson, C.T. and Hong, M. (2017) Effects of pectin molecular weight changes on the structure, dynamics, and polysaccharide interactions of primary cell walls of *Arabidopsis thaliana*: insights from solid-state NMR. *Biomacromolecules* **18**, 2937–2950 https://doi.org/10.1021/acs.biomac.7b00888

71 Thongsomboon, W., Serra, D.O., Possling, A., Hadjineophytou, C., Hengge, R. and Cegelski, L. (2018) Phosphoethanolamine cellulose: a naturally produced chemically modified cellulose. *Science* **359**, 334–338 https://doi.org/10.1126/science.aao4096

72 Romaniuk, J.A. and Cegelski, L. (2015) Bacterial cell wall composition and the influence of antibiotics by cell-wall and whole-cell NMR. *Phil. Trans. R. Soc. B* **370**, 20150024 https://doi.org/10.1098/rstb.2015.0024

73 Zhao, W., Fernando, L.D., Kirui, A., Deligey, F. and Wang, T. (2020) Solid-state NMR of plant and fungal cell walls: a critical review. *Solid State Nucl. Magn. Reson.* **107**, 101660 https://doi.org/10.1016/j.ssnmr.2020.101660

74 Wang, T., Park, Y.B., Cosgrove, D.J. and Hong, M. (2015) Cellulose-pectin spatial contacts are inherent to never-dried *Arabidopsis thaliana* primary cell walls: evidence from solid-state NMR. *Plant Physiol.* **168**, 871–884 https://doi.org/10.1104/pp.15.00665

75 Wang, T., Phyo, P. and Hong, M. (2016) Multidimensional solid-state NMR spectroscopy of plant cell walls. *Solid State Nucl. Magn. Reson.* **78**, 56–63 https://doi.org/10.1016/j.ssnmr.2016.08.001

76 Kirui, A., Ling, Z., Kang, X., Dickwella Widanage, M.C., Mentink-Vigier, F., French, A.D. et al. (2019) Atomic resolution of cotton cellulose structure enabled by dynamic nuclear polarization solid-state NMR. *Cellulose* **26**, 329–339 https://doi.org/10.1007/s10570-018-2095-6

77 Takahashi, H., Lee, D., Dubois, L., Bardet, M., Hediger, S. and De Paepe, G. (2012) Rapid natural-abundance 2D ^{13}C–^{13}C correlation spectroscopy using dynamic nuclear polarization enhanced solid-state NMR and matrix-free sample preparation. *Angew. Chem. Int. Ed.* **51**, 11766–11769 https://doi.org/10.1002/anie.201206102

78 Takahashi, H., Hediger, S. and De Paepe, G. (2013) Matrix-free dynamic nuclear polarization enables solid-state NMR ^{13}C–^{13}C correlation spectroscopy of proteins at natural isotopic abundance. *Chem. Commun.* **49**, 9479–9481 https://doi.org/10.1039/c3cc45195j

79 Takahashi, H., Ayala, I., Bardet, M., De Paepe, G., Simorre, J.P. and Hediger, S. (2013) Solid-state NMR on bacterial cells: selective cell wall signal enhancement and resolution improvement using dynamic nuclear polarization. *J. Am. Chem. Soc.* **135**, 5105–5110 https://doi.org/10.1021/ja312501d

80 Kono, H. (2004) Two-dimensional magic angle spinning NMR investigation of naturally occurring chitins: precise ^{1}H and ^{13}C resonance assignment of alpha- and beta-chitin. *Biopolymers* **75**, 255–263 https://doi.org/10.1002/bip.20124

81 Kameda, T., Miyazawa, M., Ono, H. and Yoshida, M. (2004) Hydrogen bonding structure and stability of α-chitin studied by ^{13}C solid-state NMR. *Macromol. Biosci.* **5**, 103–106 https://doi.org/10.1002/mabi.200400142

82 Sikorski, P., Hori, R. and Wada, M. (2009) Revisit of α-chitin crystal structure using high resolution X-ray diffraction data. *Biomacromolecules* **10**, 1100–1105 https://doi.org/10.1021/bm801251e

83 Yui, T., Taki, N., Sugiyama, J. and Hayashi, S. (2007) Exhaustive crystal structure search and crystal modeling of beta-chitin. *Int. J. Biol. Macromol.* **40**, 336–344 https://doi.org/10.1016/j.ijbiomac.2006.08.017

84 Lewandowski, J.R., De Paepe, G., Eddy, M.T. and Griffin, R.G. (2009) ^{15}N–^{15}N proton assisted recoupling in magic angle spinning NMR. *J. Am. Chem. Soc.* **131**, 5769–5776 https://doi.org/10.1021/ja806578y

85 De Paepe, G., Lewandowski, J.R., Loquet, A., Bockmann, A. and Griffin, R.G. (2008) Proton assisted recoupling and protein structure determination. *J. Chem. Phys.* **129**, 245101 https://doi.org/10.1063/1.3036928

86 Donovan, K.J., Jain, S.K., Silvers, R., Linse, S. and Griffin, R.G. (2017) Proton-assisted recoupling (PAR) in peptides and proteins. *J. Phys. Chem. B* **121**, 10804–10817 https://doi.org/10.1021/acs.jpcb.7b08934

87 Dubroca, T., Smith, A.N., Pike, K.J., Froud, S., Wylde, R., Trociewitz, B. et al. (2018) A quasi-optical and corrugated waveguide microwave transmission system for simultaneous dynamic nuclear polarization NMR on two separate 14.1 T spectrometers. *J. Magn. Reson.* **289**, 35–44 https://doi.org/10.1016/j.jmr.2018.01.015

88 Viger-Gravel, J., Lan, W., Pinon, A.C., Berruyer, P., Emsley, L., Bardet, M. et al. (2019) Topology of pretreated wood fibers using dynamic nuclear polarization. *J. Phys. Chem. C* **123**, 30407–30415 https://doi.org/10.1021/acs.jpcc.9b09272

89 Perras, F.A., Luo, H., Zhang, X., Mosier, N.S., Pruski, M. and Abu-Omar, M.M. (2017) Atomic-level structure characterization of biomass pre- and post-lignin treatment by dynamic nuclear polarization-enhanced solid-state NMR. *J. Phys. Chem. A* **121**, 623–630 https://doi.org/10.1021/acs.jpca.6b11121

90 Quinn, C.M., Wang, M.Z., Fritz, M.P., Runge, B., Ahn, J., Xu, C.Y. et al. (2018) Dynamic regulation of HIV-1 capsid interaction with the restriction factor TRIM5 alpha identified by magic-angle spinning NMR and molecular dynamics simulations. *Proc. Natl. Acad. Sci. U.S.A.* **115**, 11519–11524 https://doi.org/10.1073/pnas.1800796115

91 Gupta, R., Lu, M.M., Hou, G.J., Caporini, M.A., Rosay, M., Maas, W. et al. (2016) Dynamic nuclear polarization enhanced MAS NMR spectroscopy for structural analysis of HIV-1 protein assemblies. *J. Phys. Chem. B* **120**, 329–339 https://doi.org/10.1021/acs.jpcb.5b12134

92 Sergeyev, I.V., Day, L.A., Goldbourt, A. and McDermott, A.E. (2011) Chemical shifts for the unusual DNA structure in Pf1 bacteriophage from dynamic-nuclear-polarization-enhanced solid-state NMR spectroscopy. *J. Am. Chem. Soc.* **133**, 20208–20217 https://doi.org/10.1021/ja2043062
93 Azais, T., Von Euw, S., Ajili, W., Auzoux-Bordenave, S., Bertani, P., Gajan, D. et al. (2019) Structural description of surfaces and interfaces in biominerals by DNP SENS. *Solid State Nucl. Magn. Reson.* **102**, 2–11 https://doi.org/10.1016/j.ssnmr.2019.06.001
94 Goldberga, I., Li, R., Chow, W.Y., Reid, D.G., Bashtanova, U., Rajan, R. et al. (2019) Detection of nucleic acids and other low abundance components in native bone and osteosarcoma extracellular matrix by isotope enrichment and DNP-enhanced NMR. *RSC Adv.* **9**, 26686–26690 https://doi.org/10.1039/C9RA03198G
95 Chow, W.Y., Li, R., Goldberga, I., Reid, D.G., Rajan, R., Clark, J. et al. (2018) Essential but sparse collagen hydroxylysyl post-translational modifications detected by DNP NMR. *Chem. Commun.* **54**, 12570–12573 https://doi.org/10.1039/C8CC04960B
96 Lu, M.M., Wang, M.Z., Sergeyev, I.V., Quinn, C.M., Struppe, J., Rosay, M. et al. (2019) ^{19}F dynamic nuclear polarization at fast magic angle spinning for NMR of HIV-1 capsid protein assemblies. *J. Am. Chem. Soc.* **141**, 5681–5691 https://doi.org/10.1021/jacs.8b09216
97 Jaudzems, K., Bertarello, A., Chaudhari, S.R., Pica, A., Cala-De Paepe, D., Barbet-Massin, E. et al. (2018) Dynamic nuclear polarization-enhanced biomolecular NMR spectroscopy at high magnetic field with fast magic-angle spinning. *Angew. Chem. Int. Ed.* **57**, 7458–7462 https://doi.org/10.1002/anie.201801016
98 Smith, A.N., Marker, K., Hediger, S. and De Paepe, G. (2019) Natural isotopic abundance ^{13}C and ^{15}N multidimensional solid-state NMR enabled by dynamic nuclear polarization. *J. Phys. Chem. Lett.* **10**, 4652–4662 https://doi.org/10.1021/acs.jpclett.8b03874
99 Smith, A.N., Marker, K., Piretra, T., Boatz, J.C., Matlahov, I., Kodali, R. et al. (2018) Structural fingerprinting of protein aggregates by dynamic nuclear polarization-enhanced solid-state NMR at natural isotopic abundance. *J. Am. Chem. Soc.* **140**, 14576–14580 https://doi.org/10.1021/jacs.8b09002
100 Marker, K., Paul, S., Fernandez-de-Alba, C., Lee, D., Mouesca, J.M., Hediger, S. et al. (2017) Welcoming natural isotopic abundance in solid-state NMR: probing pi-stacking and supramolecular structure of organic nanoassemblies using DNP. *Chem. Sci.* **8**, 974–987 https://doi.org/10.1039/C6SC02709A
101 Kang, X., Zhao, W., Dickwella Widanage, M.C., Kirui, A., Ozdenvar, U. and Wang, T. (2020) CCMRD: a solid-state NMR database for complex carbohydrates. *J. Biomol. NMR*. https://doi.org/10.1007/s10858-020-00304-2